

Time domain passive seismic processing at Valhall

Brad Artman

ABSTRACT

Passive recordings from an array of 2500 four component receiver stations at the Valhall reservoir in the Norwegian North Sea were made available from February 2004 and January 2005 by BP. Analysis of some of the raw hydrophone records shows that the bulk of the records do not yield obvious, crisp events. Some noise trains that look like approximately 7 second envelopes of a shot record emanating from the location of the production/drilling facilities are observed occasionally. Crisp water-velocity hyperbolic events are sometimes seen which are also centered at the location of the platforms within the array.

Simple correlation does not yield interpretable synthesized shot gathers from the raw data. Dividing the correlations by the power spectrum of the traces correlated reveals several interesting features. There are a few complete hyperbolas in the data that may correspond to the desired events analogous to active seismic data. Dominating the gathers however, is a single event from a source probably 40 km to the West of the array traveling at roughly 1450 m/s. The same event is present in both the 2004 and 2005 data. The event locus is exactly over the Ardmore field in British waters, operated by Tuscan Energy (Scotland) Limited.

INTRODUCTION

BP, with partners Hess, Shell, and Total, has donated approximately 43 hours of continuous passive seismic records from the permanent sensor installation above the Valhall reservoir in the Norwegian North Sea. Figure 1 is a map of the Norwegian oil infrastructure around the Valhall reservoir between the coasts of England and Norway showing the many developments in the region. It is 630 km from the Southern tip of the Norway shown and the city of Teeside in England.

There are five surface structures (roughly over the center of the reservoir), and two well-head platforms at the North and South ends of the NW-SE elongate elliptical reservoir (both roughly 6 km from the central platforms). The main fluid export pipeline runs NNW to the Ekofisk reservoir, about 30 km distant. Figure 2 shows the location of the 13 lines of OBC 4C geophones installed in the summer of 2003. The +10,000 sensors are permanently installed on the sea floor, in roughly 70 m of water, forming a roughly 5 by 10 km rectangle. Nominal in-line spacing of receiver stations is 50 m, while the cross-line separation is 300 m.

Approximately half-way down the North axis of Figure 2, the cables on the Western side

Figure 1: English, Norwegian, and Danish coasts surrounding the North Sea oil development area. The Valhall reservoir is in the South-central area of the map and only 20 km from English-controlled waters to the West, and Danish waters to the South. areamap [NR]

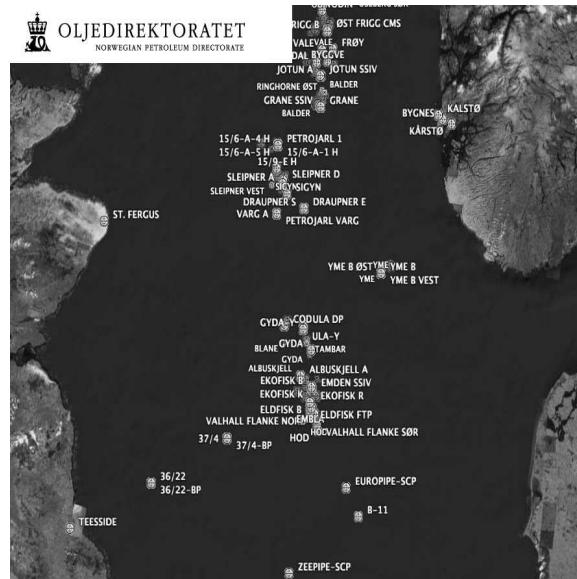
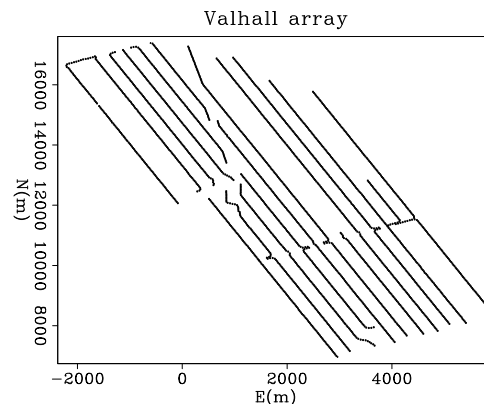


Figure 2: Valhall permanent subsea geophone array. Each station measures 4 components (4C) of the seismic wavefield: Pressure with a piezoelectric sensor, and three orthogonal velocities of ground displacement with coil-spring geophones. actg [NR]



of the array are truncated. This is where the production facilities are located to which the instruments are telemetered. Also noticeable is the deviation of the ends of cables on the North side of lines 5-7 ($E=1000\text{m}$) to the NNW. This is the corridor for the export lines to Ekofisk. Production facilities are continuously manned and operated, to include: Over 150 total well-bores into the reservoir section, current production of approximately 80,000 b/d oil and gas from 43 wells, water injection through (at least) 3 wells, generation of almost 80 MW of electrical power with gas turbines, export lines and the continual presence of multiple modes of transportation¹. Valhall is located in a heavily developed area, within kilometers of developments in the English and Norwegian controlled waters and is about half-way between the two countries. Also important to the chalk oil trend of this part of the North Sea is the rate of subsidence associated with pressure withdraw during production. In its first 15 years of production (to 1997), the sea-floor subsided 3.5 meters at the crest of the reservoir structure (Gebara et al., 2000).

¹www.npd.no/engelsk/

PASSIVE SEISMIC RECORDING

Passive recordings were made available from 30 hours February 15, 2004, and 14 hours January 19, 2005. Of the former, some 7 hours was lost due to a failed disk-drive. Of the 2500 4C stations, this work uses the hydrophone measurement from each location. The data are sampled at 0.004 ms, and recorded as contiguous files approximately 15 seconds long. Figure 3 shows an example of the character of much of the data. The traces were balanced against each other, but are otherwise raw recordings.

Figure 4 shows a conspicuous noise-train in a section of raw data. While there are no coherent events, a noise-train about 7 seconds long within the background chatter is reminiscent of the envelope of a shot-gather. The minimum travel time of the noise-train is at trace 650. This trace is located at the end of the top half of the fourth receiver line. The various jogs and cable terminations of this region are associated with the surface facilities on location. Plotted over the data are time picks modeled as a direct arrival from the location of the platforms in the plane of the receivers. These were shifted to align with the top and bottom of the noise train. The velocity used to model this event is 1450 m/s. The fact that there is no velocity increase for the bottom of the envelope suggests that this feature does not contain reflections from the subsurface. Similar examples of this type of noise-train are periodically recognizable throughout data recordings. The source of the energy has a complex coda and a finite duration.

Figure 5 shows a short time window when a crisp series of hyperbolic events is captured by the array. The top panel is the Eastern half of the array and the bottom is the Western half. The minimum travel-time of the hyperbolas decreases to the West of the top panel in a similar fashion to the onset of the noise section in the previous figure. This suggests that the production facilities are again the source of the energy. The time picks overlaying the data in Figure 5 are the kinematics of a co-planar direct arrival from the 'O' in Figure 6 traveling at 1450 m/s. Every third pick was plotted to avoid clutter. However, even when plotting all picks in high resolution, the forward modeling clearly shows that the data are aliased at this slowness value over the center of the array where the event is not visible. Similar events are recognizable throughout the records, though this is a particularly clear example.

Figure 6 is a map of the array rotated to convenient field coordinates. The 'X' symbols mark the locations of the traces with minimum hyperbolic travel-times that were obvious in the previous figures. The line containing the minimum travel-time picks shows no inline offset variation and includes the area around $y = 6250$ m, which is the location of the platforms (presumably near the 'O' symbol). This figure provided the inline location for the picks plotted in Figures 4 & 5. The crossline coordinate was deduced by matching the picks to the various observations.

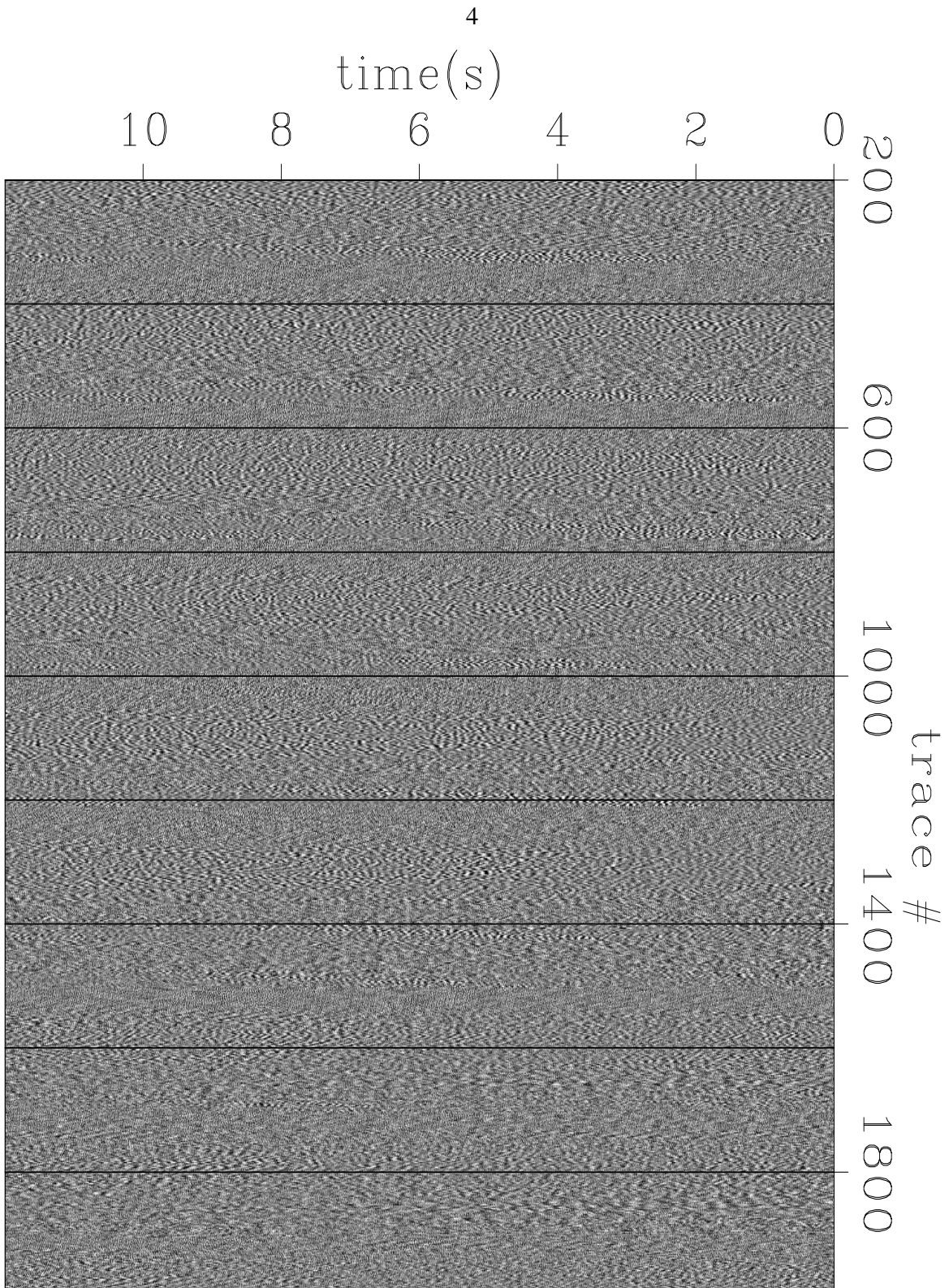


Figure 3: Twelve seconds of representative passive hydrophone data from February 16, 2004. Trace number increases from the top left to bottom right corners of the array shown in Figure 2.

`raw1` [ER]

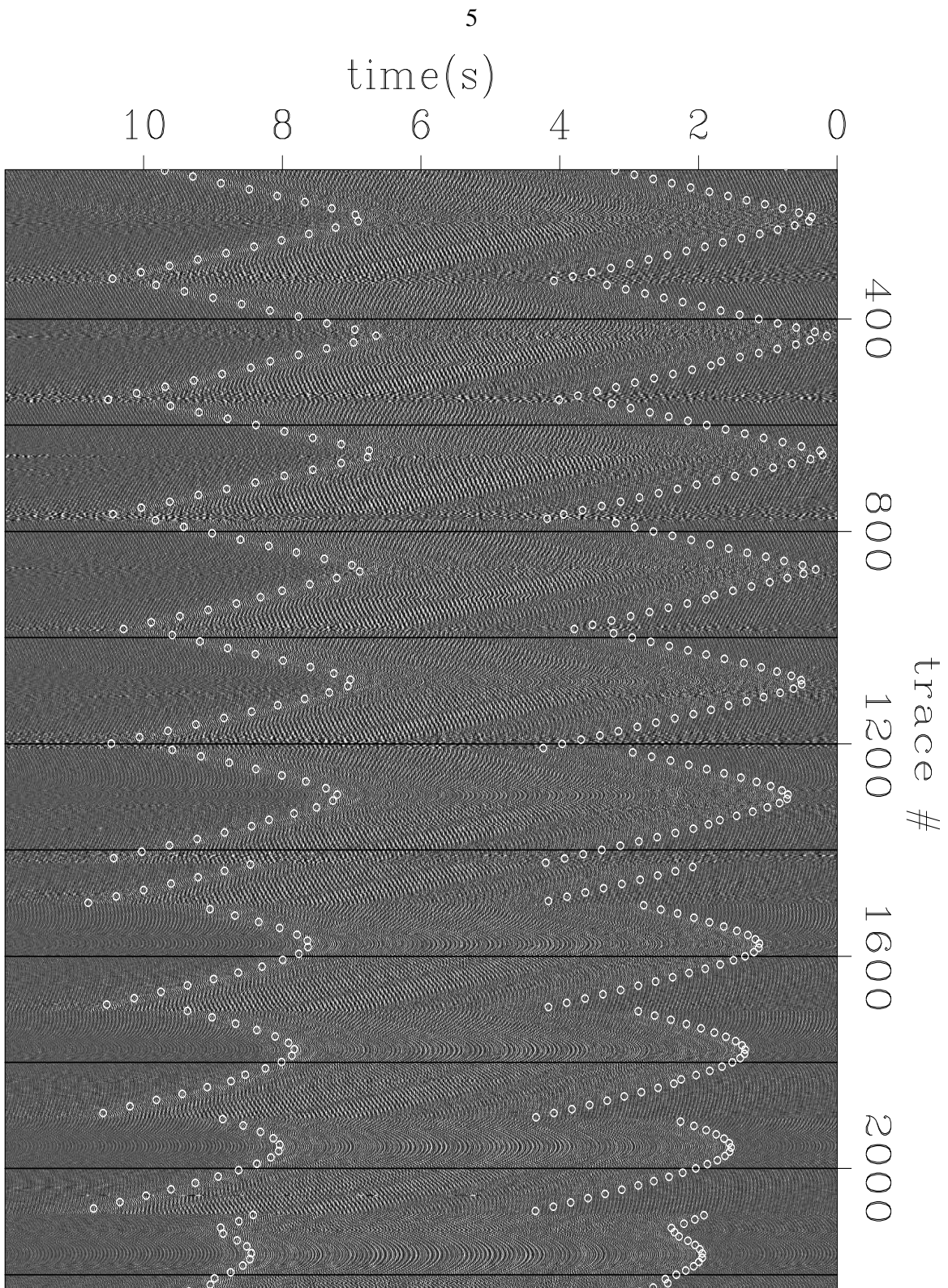


Figure 4: Raw data with a powerful noise train envelope. The 13 lines of the array show as the event is repeated and shifted over cross-line offset. The picks are co-planar direct arrivals from the center of the array traveling at 1450 m/s. `raw2` [ER]

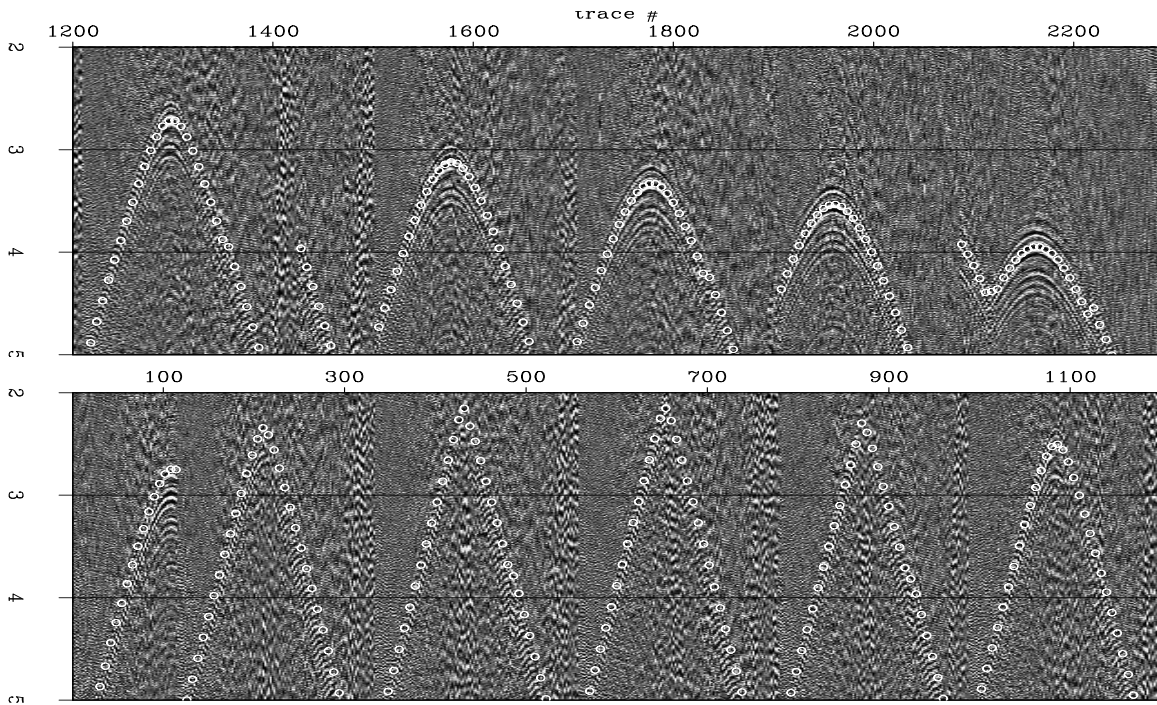
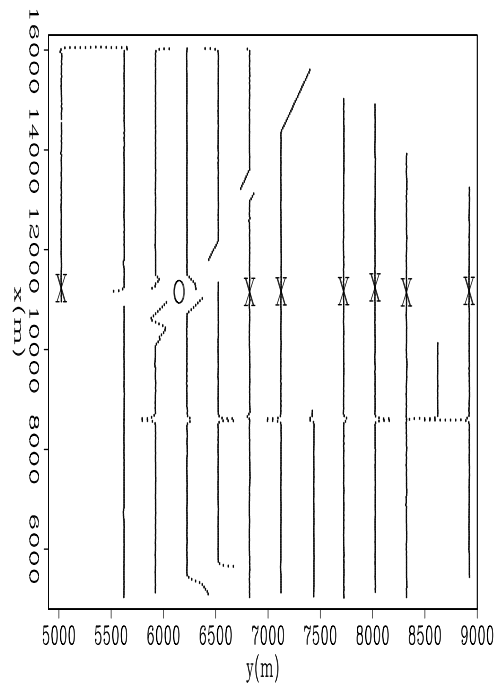


Figure 5: Raw data with a clear hyperbolic event and time picks calculated for a coplanar direct arrival from the array center traveling at 1450 m/s are. `raw3ev` [ER]

Figure 6: Receiver array in field coordinates. Marked with 'X' are the locations of traces with minimum travel-times picked from the hyperbolas in Figure 5. Even though the event is not clear on the central lines of the array, the line connecting the traces where it is visible intersects the location of the surface facilities. `minloc` [ER]



CORRELATION

Following the theory from Wapenaar et al. (2004), the basic principle of time processing passively recorded seismic records to yield the kinematics of actively collected data dictates

$$2\Re[R(\mathbf{x}_r, \mathbf{x}_s, \omega)] = \delta(\mathbf{x}_s - \mathbf{x}_r) - \int_{\partial D_m} T(\mathbf{x}_r, \boldsymbol{\xi}, \omega) T^*(\mathbf{x}_s, \boldsymbol{\xi}, \omega) d^2 \boldsymbol{\xi}, \quad (1)$$

where $*$ represents conjugation. The vector \mathbf{x} corresponds to horizontal coordinates, where subscripts r and s indicate different station locations from a transmission wavefield T . After correlation, r and s acquire the meaning of receiver and source locations, respectively, associated with an active survey. The RHS represents summing correlations of windows of passive data around the occurrence of individual sources from locations $\boldsymbol{\xi}$. The symbol ∂D_m represents the domain boundary that surrounds the subsurface region of interest on which the sources are located. The transmission wavefields $T(\mathbf{x}_r, \boldsymbol{\xi}, \omega)$ contain the arrival and reverberations due to a single subsurface source. To synthesize the reflection experiment exactly, impulsive sources should completely surround the volume of the subsurface one is trying to image. Alternatively, many impulses can be substituted with a full suite of planewaves emerging from all angles and azimuths.

Because windowing individual arrivals from the 79 Gbytes of data associated with the hydrophone measurement is impractical, it is impossible to honor equation 1 precisely by correlating traces within time windows when only a single event is active. However, this effort makes the assumption that processing data in 12 second sections is a reasonable approximation to the requirement. The available data were divided into three sections for processing: one 13.5 hours, two 9 hours, and one 4.5 hours in duration. Sequential 12 second records from all the stations were correlated in accordance with equation 1 and the results stacked over the duration of the (hours long) section of available data. Thus

$$\hat{R}(\mathbf{x}_r, \mathbf{x}_s, \omega) = \sum_{\xi} T(\mathbf{x}_r, \omega, \xi) T^*(\mathbf{x}_s, \omega, \xi) \quad (2)$$

was calculated where ξ is the set of sequential 12 second chunks of data.

Figure 7 shows correlations from one of the 9 hour sections of data. A trace from the NW corner was used to correlate all the other traces in the array. If the processing was perfect, the figure would show something equivalent to an off-end areal shot-gather. Energy to 60 Hz energy was used in the correlations, with cosine tapers beginning at 3 and 57 Hz. Unfortunately, the image, and the other similar ones, do not reveal anything of interest. Figure 8 plots the power spectrum of the sum of 100 traces from the gather in Figure 7. Versions of the data bandpassed around and between the peaks made no appreciable increase in interpretability.

Spectral whitening by division of a trace in the frequency domain with its power produces remarkable results when compared to simple correlation. Gathers were also produced using the relation

$$\hat{R}(\mathbf{x}_r, \mathbf{x}_s, \omega) = \sum_{\xi} \frac{T(\mathbf{x}_r, \omega, \xi) T^*(\mathbf{x}_s, \omega, \xi)}{\|T(\mathbf{x}_r, \omega, \xi) T^*(\mathbf{x}_s, \omega, \xi)\|}. \quad (3)$$

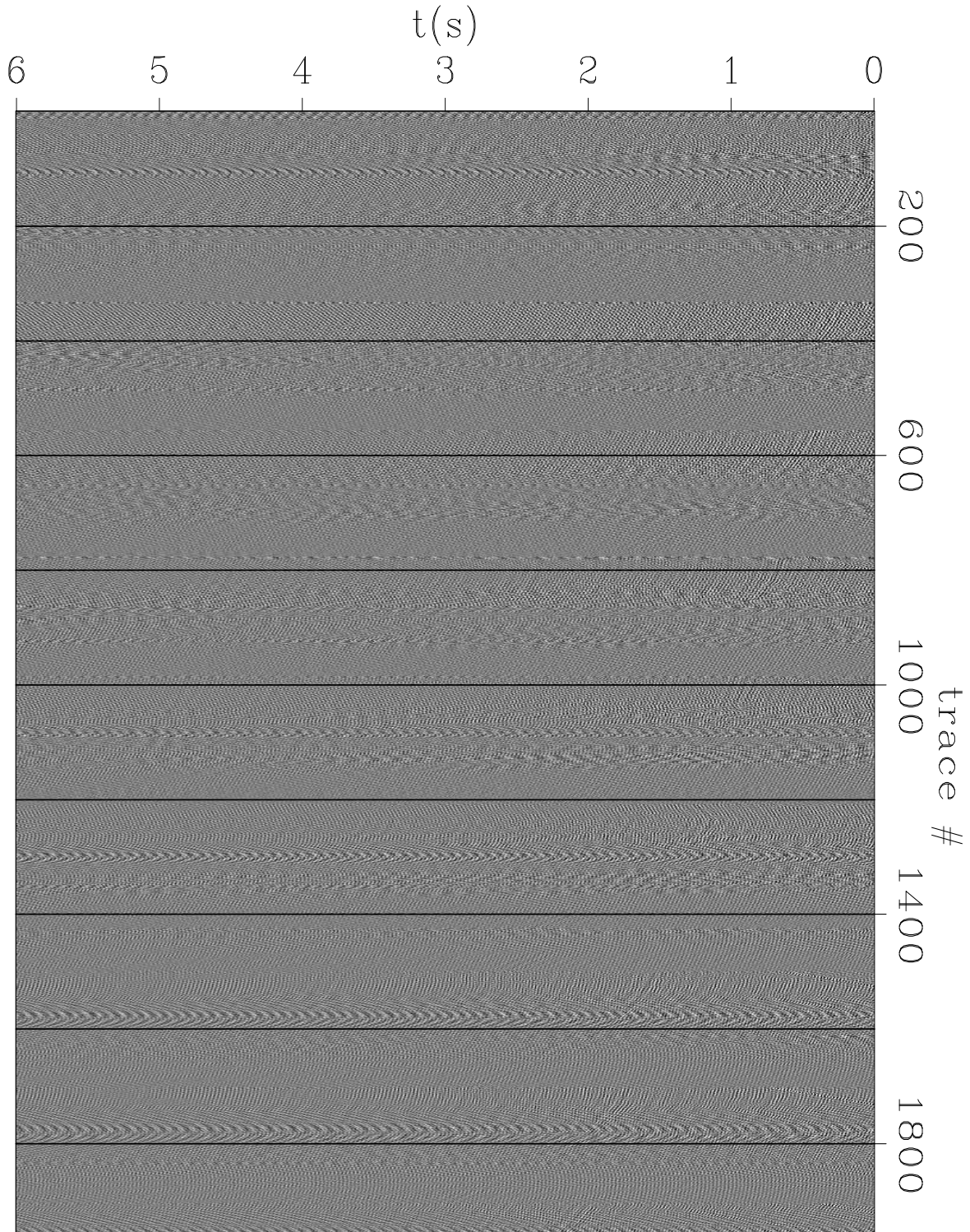
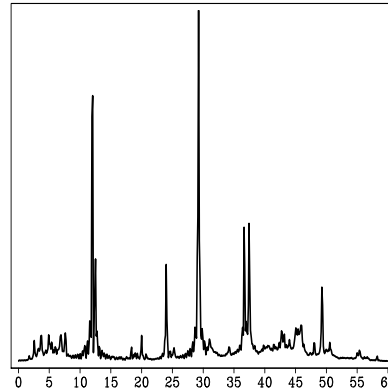


Figure 7: Correlated shot-gather with source location at the left side of the panel. 0-60 Hz energy was used for the correlation performed in the frequency domain. cor [ER]

Figure 8: Power spectrum of the gathers in Figure 7. `spec` [ER]



The algorithm was very stable and showed no need to smooth the denominator as is common practice in similar deconvolutional efforts. In fact, smoothing the denominator across the trace axis produced large amounts of hard zero results. This can only be explained by large amplitude, uncorrelated energy on neighboring traces. Dividing a weak sample by a very strong neighbor will produce very small values. Smoothing across the frequency axis mixes early- and late-time energy, and therefore is not appropriate.

Figure 9 shows the same gather as in Figure 7 using the spectral whitening of equation 3. A very clear event is now apparent. Similar features can be seen upon close inspection of the correlated result after viewing the deconvolved gather. The various features of the obvious event in the gather reveal important features of the presumed source energy. The event is coherent across the entire 50 km² of the array and has reasonable bandwidth. Versions of data were bandpassed across the intervals between and surrounding the energy maximums in power spectrum, Figure 8, of the correlated gathers. No coherent energy was present at all through 8 Hz. Five versions from 9-40 Hz showed only minor differences, with the strong event equally well represented. After 42 Hz, the signal begins to diminish markedly, and no coherent energy is present at all after 52 Hz.

Events are hyperbolic. This indicates the event could be caused by any solution to the class of hyperbolic PDE's. Possible solutions include the direct arrival of a buried source, or the reflection of a point source from a plane. No line contains the top of the hyperbola. This means that the source of the energy is not contained within the area of the array. The moveout of the event is monotonic to the South and East. This indicates that the source must be to the North and West. Moveout is curve-linear in the inline direction, but very close to linear in the cross-line direction. The line connecting the minimum travel-times of the event on each cable deviates from straight only at the far right side. Notice from the map in Figure 6 that crossline offset there is twice the normal spacing. This indicates that the array is close to the asymptotic limit of the hyperbolic event in the cross-line direction, and nearer the hyperbola top in the inline direction. These two observations indicate that the source is much closer to the array in the inline direction than the perpendicular direction. Given the true geographical orientation of the array, Figure 2, the source of energy should be somewhere West of the location toward the English coast.

The fact that the event does not contain the center of the hyperbola, proves that processing

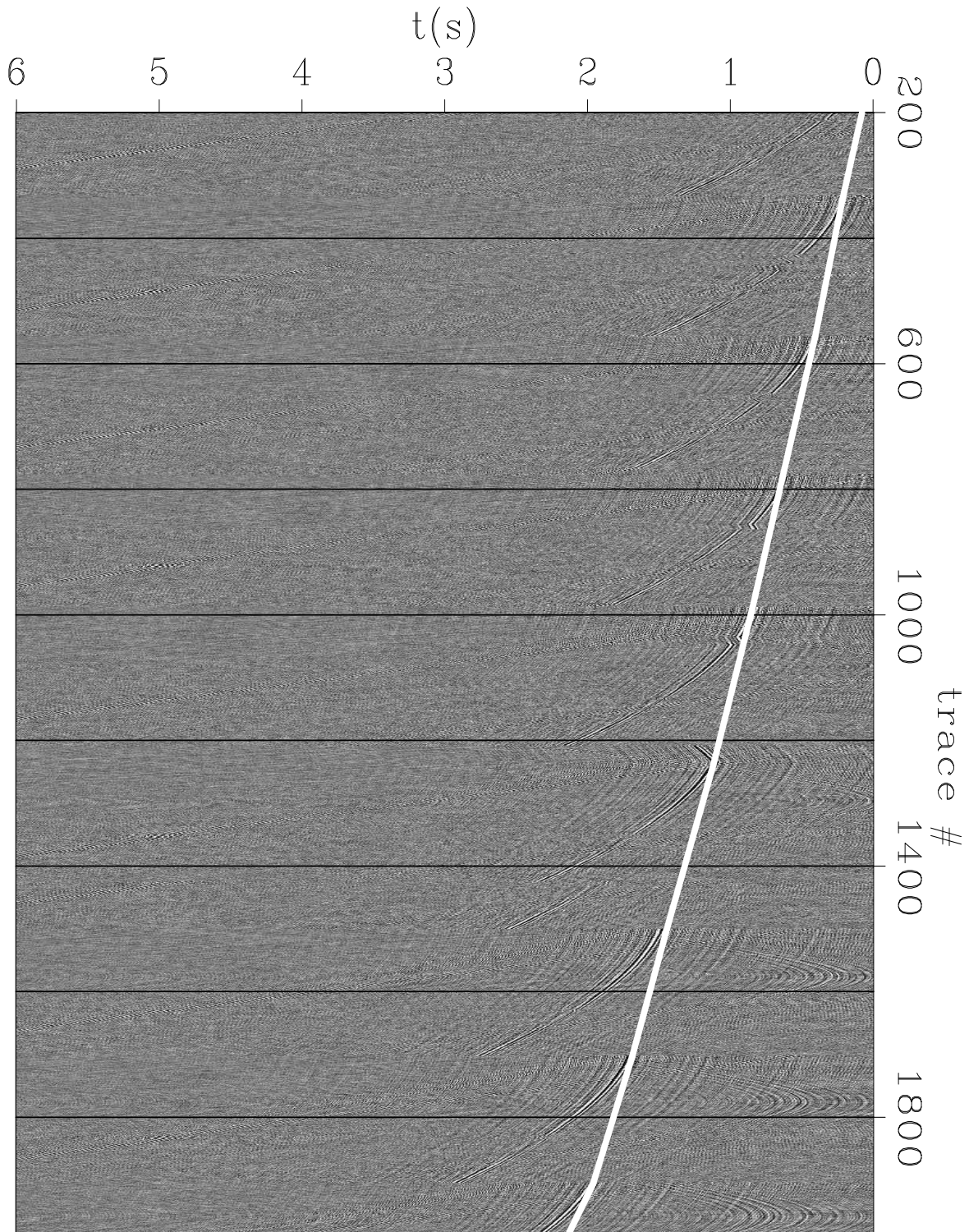


Figure 9: Trace-by-trace spectral whitening applied to shot-gather in Figure 7. Line connecting minimum travel-times almost perfectly straight. dec [ER]

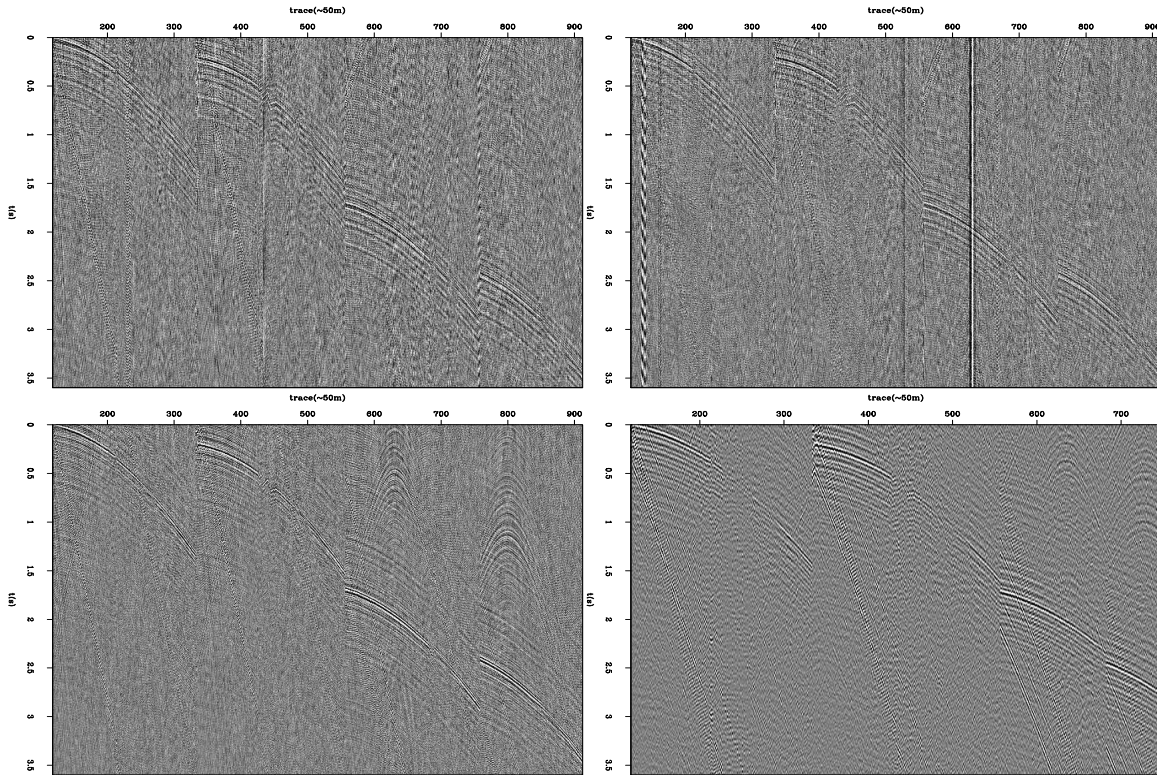


Figure 10: Ubiquitous strong event in correlated and deconvolved shot-gathers from data recorded 9 hours, 25 hours, and 11 months after that used to produce the first panel. The third panel is a subset of the gather shown in Figure 9. event [CR]

by correlation to produce conventional shot-gathers has failed. Specifically the requirement to sum the correlations from many shots in equation 1 has not been honored. If only a single shot is captured by a passively recorded array, correlation simply shifts the event up such that it arrives at $t = 0$ at the source-trace used to create the gather. The moveout of the event will not be altered at all. I believe the energy is localized in space, but seemingly ubiquitous in time. Figure 10 shows four lines from the array from the same correlated shot-gather from the four time periods into which the data volume was divided. The lines are the first and last two complete receiver lines from Figure 6. The third panel is a subset of the gather shown in Figure 9. Each trace was correlated with the first trace in the panel. Thus the event on the autocorrelated trace is at time zero. Some of the character of the panels changes, but the presence and kinematics of the obvious energy is the same. The last panel was computed with data recorded almost one year after the data used in the first three panels.

Figure 11 shows four synthesized shot-gathers using data shown in the previous section concerning the character of the raw recordings. The source trace used for correlation in all panels was the first trace on North end of line 2 (trace 119). All panels use the deconvolutional variant of correlation described by equation 3 and show the Eastern side of the array. The first panel is the first three seconds of the causal lags using the data shown in Figure 4 which showed the ringing noise-train. No strong events are present, but there are some faint ringing

hyperbolas that show water velocity.

Correlation subtracts the time to the source trace from all the other traces in the gather. The beginning of the noise-train in Figure 4 on the first trace (number 119), is at about 3.5 s. The top of the noise train on the last receiver line (trace number 2150) is at about 2 s. The complicated coda evident in the raw data should collapse to a simple wavelet during correlation. Therefore, we expect the top of the energy on the last receiver line to lie at about -1.5 s. The acausal lags in the second panel of Figure 11 show exactly what was expected. Overlain on the correlated event are time picks modeled with the same 1450 m/s arrival used to delineate the noise-train in Figure 4. The hyperbolas ring to the bottom ($t = 0$) of the panel. Given the long (7 s) coda of the noise train, these are probably correlation side-lobes that are also responsible for the events seen in the panel to its left.

The bottom row of Figure 11 are the deconvolved correlated gathers using trace 119 as a source and the data from Figures 3 & Figure 5 respectively. In each case only 12 s of data were correlated. Faint hyperbolas are discernible in the early time of the right side of the right panel. The most obvious energy however is in the events similar to the strong arrivals in Figure 9 and Figure 10.

Correlation masks some of the characteristics of the source energy. The source could be impulsive or a long sweep containing many frequency components like a vibrator source. The latter seems less likely. The source could be a single strong event, or many similar repeated events with low amplitude. Given the presence of the event during all the time intervals in Figure 10, I favor the latter explanation.

Figure 12 shows the same correlated gathers as Figure 10. Superimposed on the data are time picks that were auto-picked by amplitude. The picks are not very accurate due to the effort required to maintain stability. These picks, and the receiver locations, are the data used to invert for the source location that caused these events. The forward model used for the inversion was the kinematics of a reflection from an arbitrary plane. Inversions for a direct arrival from depth were not successful.

The equation describing the travel-time of a planar reflection in shot-receiver coordinates is

$$v^2 t^2 = \mathbf{x}^2 + 4z^2 + 4z\mathbf{x} \cos \alpha \sin \phi \quad (4)$$

where \mathbf{x} is the map distance from the source to the receiver, z is the depth of the plane under the source location, α is the azimuth of the line \mathbf{x} minus the dip direction of the plane, and ϕ is the dip of the plane. At the limit of $z = 0$, the operator solves for a co-planar direct arrival. Correlating the data with a single source trace subtracts the time to the source trace from each trace in a gather. Therefore, the forward modeling operator used in the inversion solves for the time, t_s , to the source-trace location using equation 4 and subtracts this value from each trace in the shot-gather to produce the time differences produced in a correlated panel. Subtracting t_s in the forward modeling operator greatly diminishes the operator's sensitivity to the terms on the RHS involving depth. Also, large horizontal distance will result in the first term, \mathbf{x}^2 , to dominate the others. The inversion technique used was a micro-genetic algorithm. The model space is: Average velocity through which the rays have passed, areal location of the source, and orientation angles and depth of the reflection plane. The fitness function for the genetic

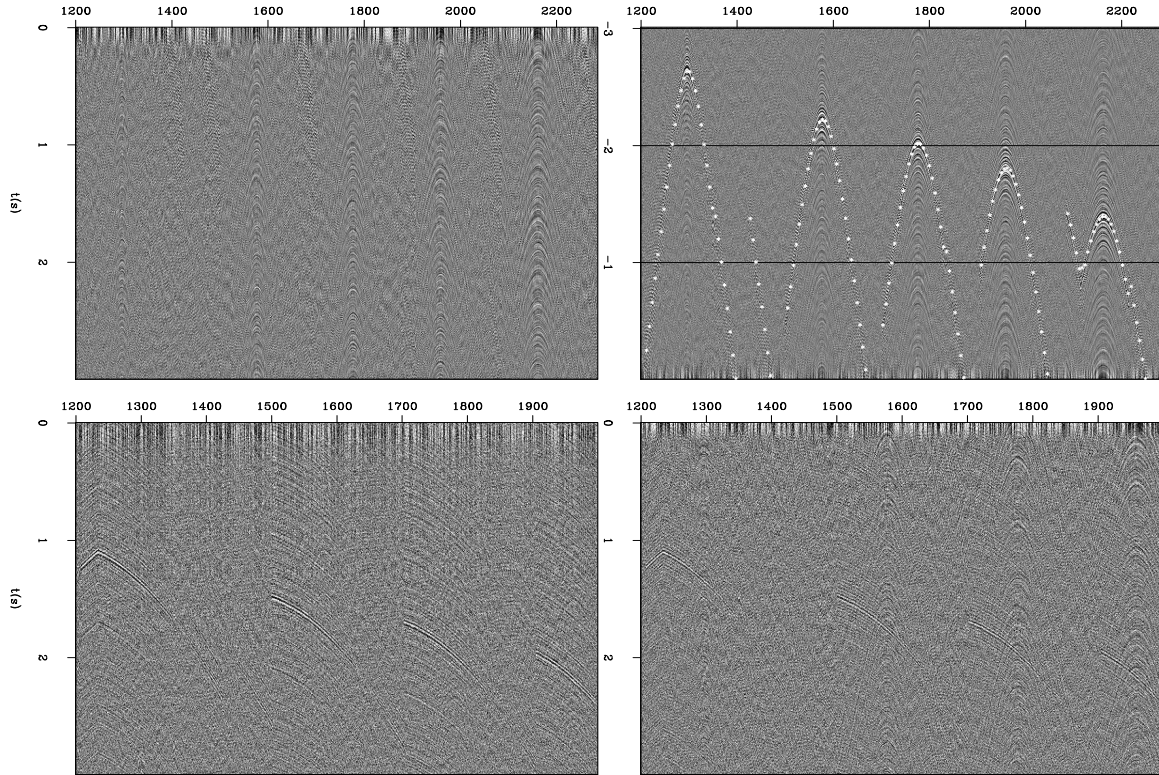


Figure 11: Correlated gathers from the Eastern side of the array. Top row: Early causal and acausal lags of a correlated gather using data in Figure 4. Picks on right panel have same (1450 m/s) velocity and origin as those delineating the top and bottom boundaries of the raw data. Bottom row: Early causal lags of correlated gathers using data in Figure 3 & Figure 5. `evtest` [ER]

algorithm was the l^2 norm.

The panels in Figure 13 show the effectiveness and quality of the inversion results. The genetic algorithm uses a random seed number that determines the characteristics of the first population as well as how the future generations change. Fifteen seeds were used to find the source location and medium velocity for all four data sections. Figure 13 is a representative sample of the four inversion results. The panels in the figure show the convergence of the algorithm in total (panel 1), and the convergence of the model parameters: velocity, distance East, and distance North respectively. In each case the vertical axis is the fitness value that the inversion is minimizing. The relative width of the data cloud at the minimum fitness value for the 3 model parameters shown reflects the precision of the inversion for this data. Velocity and distance North are very well constrained, but distance East has a wide region of minimum energy. Not shown are similar plots for the model parameters associated with the planar reflection: depth, dip, and azimuth. These parameters were completely in the null space of the inversion.

Figure 14 shows the forward modeled time picks from the inversions. The best model parameters from all 15 inversions were forward modeled and plotted. The points are very

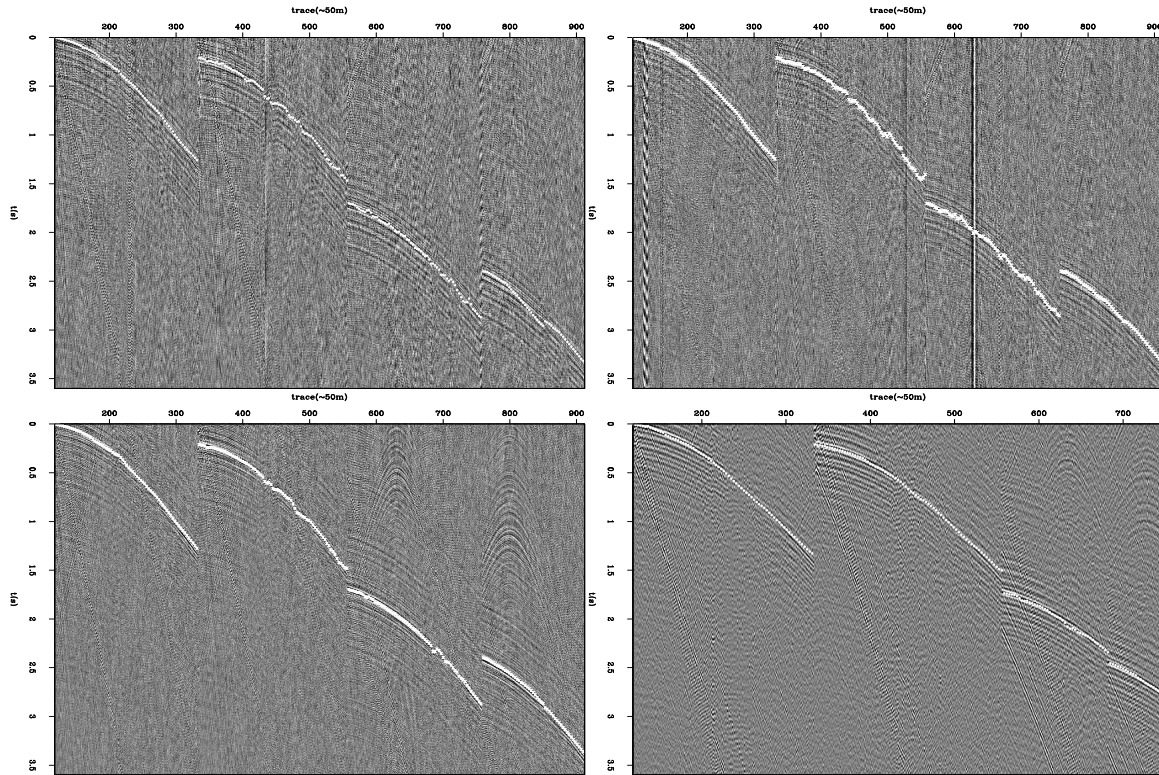
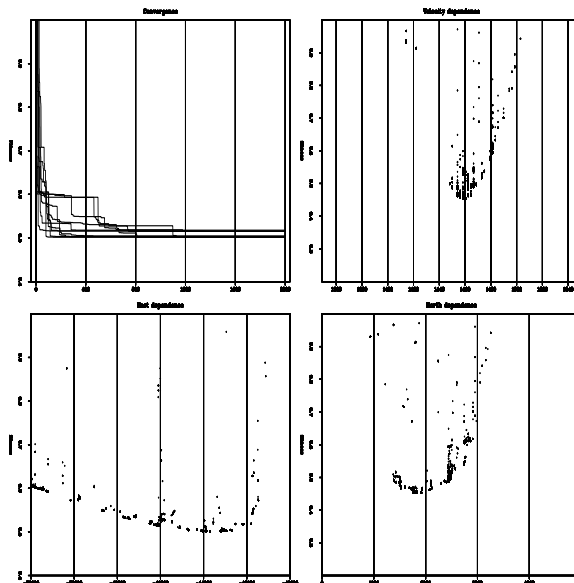


Figure 12: Auto-picked time values along event in correlated gathers. Picks are used as data when inverting for the source location. `picks` [CR]

precise in picking even minor deviations from regularity in the array geometry and are much better at describing the event than the auto-picks in Figure 12. The quality difference between the picks that went into the inversion and the result account for the residual energy in the first panel of Figure 13. The inversion was not able to match the bad data because it was required to honor the laws of physics. Therefore, the result is not able to converge to zero.

Using graphs such as those shown in Figure 13, values for map coordinates and velocity were selected at the location of the minimum from all 15 inversions. The best velocity for the three data sets from 2004 was 1460 m/s, and 1440 m/s for the data from 2005 which are appropriate for compressional waves in the water column. The (x, y) locations measured as distance from the NW corner of the array in kilometers were: (2.5, -44.0), (2.0, -40.0), (2.4, -43.5), (2.75, -43.5) in the rotated local coordinate system shown in Figure 6. Because the inversion returned very reliable water velocities in all cases, the lack of sensitivity for the subsurface parameters is mitigated. If the event must be in the water column, the sea surface and floor are the only potential reflectors. Since the receivers are on the sea floor, the most simple explanation of these results is that the source is also at the sea floor and reflects from the sea surface once before arriving at the array. However, at such large horizontal offset, and shallow water column, the forward model cannot distinguish between this model and the direct arrival from the surface to the sea floor. Conversely, the source could be at the array, travel roughly horizontally, and reflect back from a nearly vertical object. The latter situation

Figure 13: Residual energy of the inversion to locate the source of the energy causing the event in Figure 12. As the inversion iterates, overall residual energy decreases, and the standard deviation of the model parameters diminishes for well constrained members. `inv` [CR]



is not plausible, nor is the direct arrival associated with this model recorded by the array.

Using the values listed above, time picks at every receiver station were forward modeled for use as data in an exhaustive search inversion. The gray scale in Figure 15 shows the inverse of the data misfit normalized by the maximum value. The velocities used were those stated above. The same line is plotted on the panels for reference (8° from the horizontal axis). All data volumes resolve the source location at very similar locations with almost identical trends in precision. A request to the Norwegian Petroleum Directorate indicates that there were no active seismic vessels acquiring data in this region on or around February 15, 2004. The similar location derived from the data collected in 2005 indicates that surface seismic acquisition is likely not the cause of this feature.

The geometric construct used to calculate the kinematics of a reflection from a flat plane is to double the time from the source to the midpoint on the plane. It is also possible that the source location was twice the distance away and the event is a multiple along the same azimuth. Another possible ray path which shares the kinematics of the forward modeling operator is one with three ray paths through the water column. This event begins at the surface, is reflected up from the sea floor, and then once more from the surface to be recorded by the OBC sensors. This travel path is at most $2/3$ of the distance from the array along the same azimuth. Similarly, any odd number of raypaths, k , through the water column will move the source toward the array by $2/k$. Therefore, it is plausible to move the source location from the inversion almost anywhere along the azimuth of the lines plotted in Figure 15.

Figure 16 is a detailed map of the Norwegian and British oil infrastructure around the Valhall reservoir. Also plotted are the footprint of the receiver array, and the location of the trace used as source function (G118) for the gathers presented above. Superimposed as a flat image (and thereby introducing small projection errors) is a map of the British production facilities in the area. The black line from the receiver array ends in the SW at the locus of the energy provided by the inversions described above. The location of the source for the events

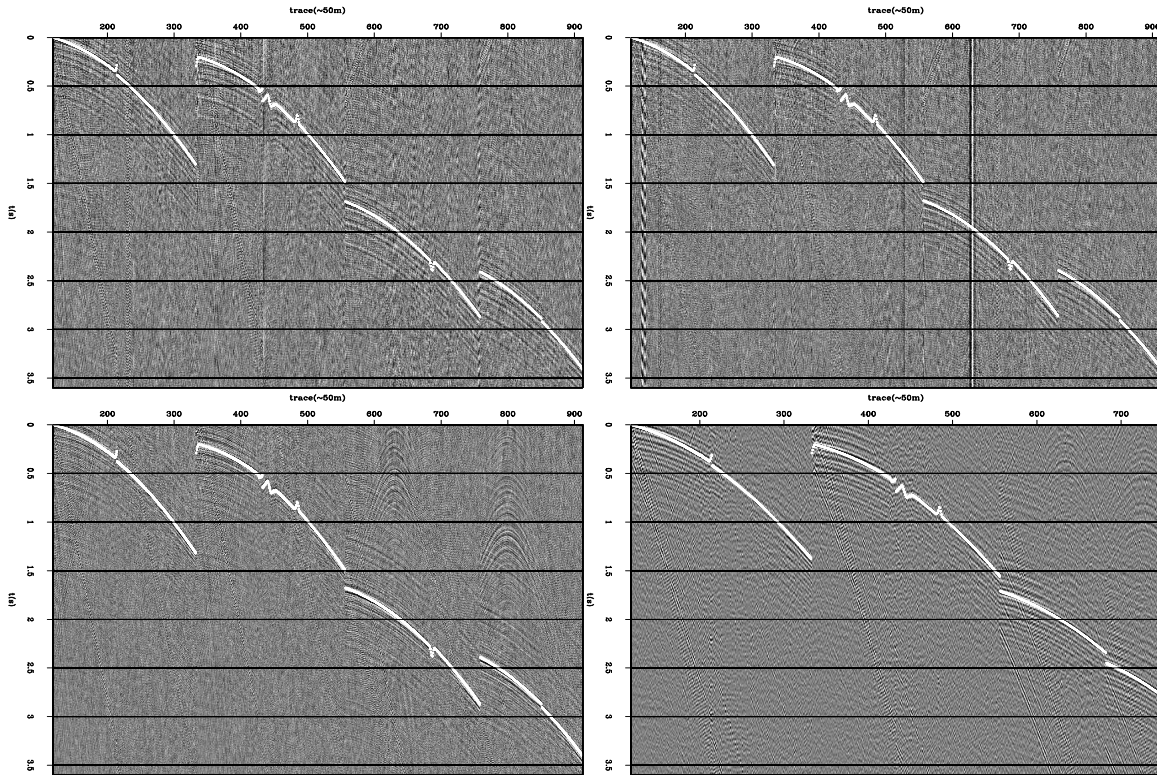


Figure 14: The forward modeled time picks from 15 inversions are plotted over each panel in Figure 10. The accuracy of the times is very faithful to the irregularities in the array layout in contrast to the auto-picked data input to the inversion, Figure 12. mods [CR]

in Figure 10 is exactly over the Ardmore field in British controlled section of the North Sea.

CONCLUSIONS

The energy responsible for the features in the raw data, Figures 4 - 5, are likely related as they share a locus at the production facilities and are both characterized by water velocity. I suspect that the noise-train in Figure 4 is a collection of aliased repeating events similar that found in Figure 5. Also, the gathers generated with data showing the diffuse noise-train, Figure 4, have almost identical kinematics to the raw data showing a crisp water-velocity event, Figure 5. It is possible that some activity on the platforms could sometimes be impulsive in nature or more drawn out. In either case, the correlated gathers do not show convincing evidence that the energy penetrates the subsurface after the direct arrival is recorded. Forward modeling the direct arrival to the receiver stations shows that water velocity events are aliased close to the source with this array. This analysis of the raw data also shows that the predominance of observable energy shares a single source location.

Correlating the raw data to produce synthesized shot gathers was always performed on 12 second records. These individual results were summed from 1-2500 times to generate some

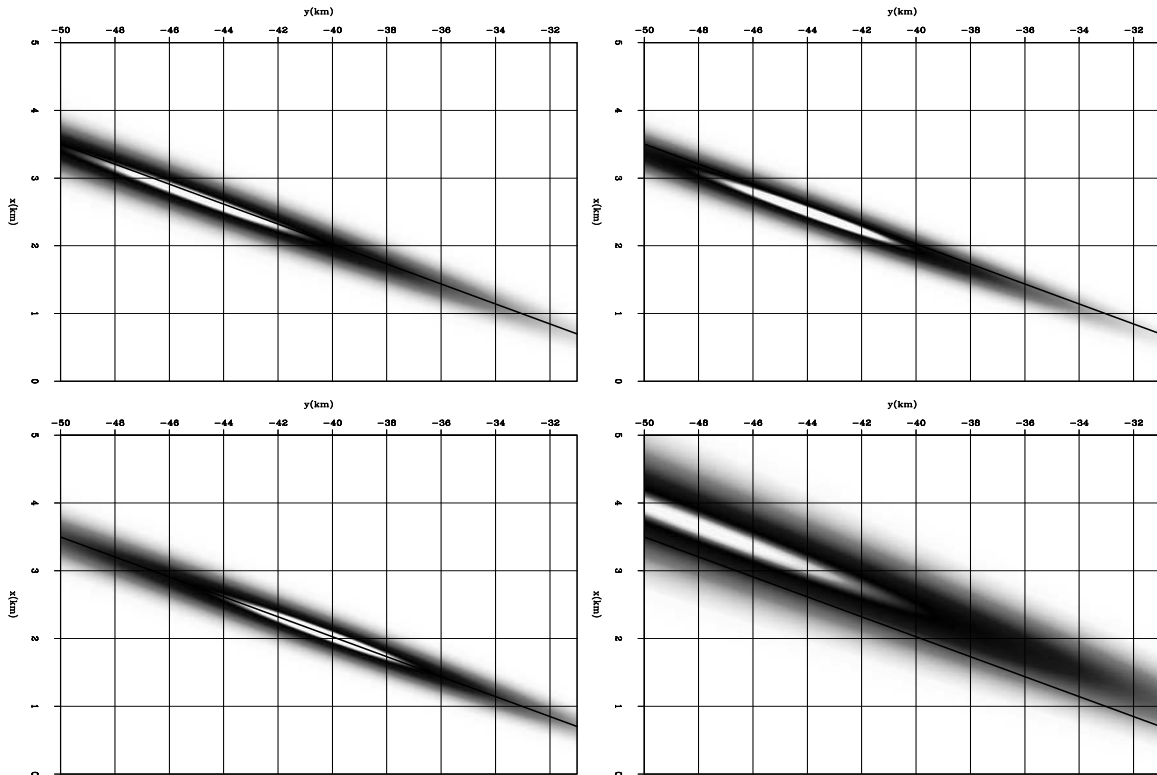
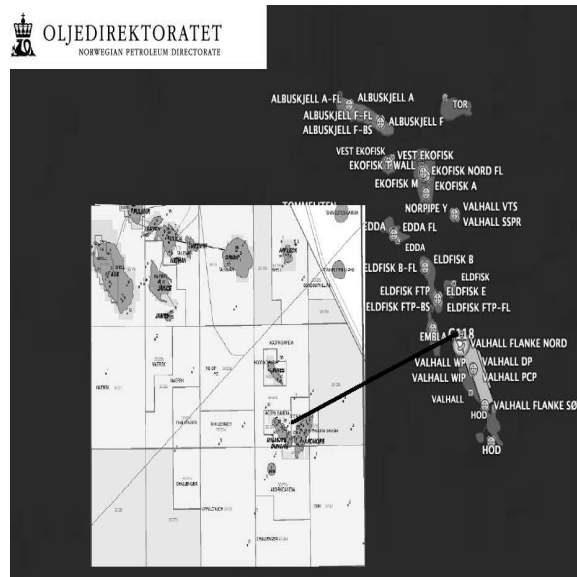


Figure 15: Sensitivity to horizontal location for the inversions using the four periods of passive data. [xy](#) [CR]

Figure 16: A small section of the British infrastructure map with the Norwegian infrastructure and the location of the energy source inverted in Figure 15. The inverted locus of the energy in the gathers (the SW terminus of the black line) corresponds exactly to the location of the Ardmore development. [mapa](#) [NR]



approximation to active seismic shot gathers in accordance with the theory of interferometric imaging. The gathers produced with a single 12 second record, Figure 11, or 15 hours of data correlated in 12 second sections, Figure 10, show an identical strong event with velocity 1450 m/s arriving from the Ardmore field 40 km to WSW. Less obvious events are also present in the gathers with locus at the Valhall production facilities in the center of the array. These events are also characterized with water velocity.

It seems counter-factual to attribute the source of this energy to a distant production operation when major production, drilling, and injection activities within the array have not generated events that match the power and bandwidth of this most obvious arrival. The British Department of Trade and Industry ² describes the Ardmore development. It differs from the Valhall operation in several important ways. The Ardmore facility has no permanent structures, nor is it connected to an export pipeline. Instead, two vessels are permanently moored over the field: One contains production facilities, the other is used to store liquids for periodic transport to shore. This operation has no way to handle produced gas and must therefore flare gaseous production to the atmosphere. I believe this is the most significant difference between the two operations, and that the gas flare is the most likely sonic source for the energy recorded at the array.

With only two main energy sources developing the events in the correlated gathers, the result does not satisfy the equation which relates passive recordings to active data acquisition. Correlating events from a single source simply moves the minimum travel-time captured by the array to zero. Constructive and destructive interference from many events are required to generate events with the kinematics of an active survey. Sorting the gathers to midpoint-offset coordinates yields completely uninterpretable CMP gathers. Similarly, further processing which assumes impulsive sources located at the trace used as source function to synthesize a gather (migration) is therefore inappropriate. However, having identified the locus of the energy in the correlated gathers, the equation describing the kinematics of the event can be used as a mute function or areal source function for further processing.

REFERENCES

- Gebara, J., D. Dolan, et al., 2000, Assessment of offshore platforms under subsidence—Part i: Approach: *Journal of Offshore Mechanics and Arctic Engineering*, **122**.
- Wapenaar, C. P. A., J. Thorbecke, and D. Draganov, 2004, Relations between reflection and transmission responses of three-dimensional inhomogeneous media: *Geophysical Journal International*, **156**, 179–194.

²www.og.dti.gov.uk/environment/permits/TuscanArdmore.htm